개별 블레이드 제어 기법을 이용한 동축 반전 회전익 항공기의 진동 저감 연구

Vibration Reduction Study of Lift-offset Coaxial Rotorcraft Using Individual Blade Pitch Control

Abstract

본 연구에서는 고속 전진 비행 조건에서 개별 블레이드 조종 (IBC)을 활용한 동축 반전 회전익 항공기의 진동 저감 연구를 수행했다. 회전익 항공기의 진동 해석 모델은 동축 반전 로터와 동체를 포함한다. 동체 모델은 XH-59A 및 여러 헬리콥터의 실제 고유진동수를 참고하여 유한 요소 모델링을 수행하였다. 로터-동체 연계 해석 수행을 위해 고유진동수 모드에 따른 동체의 진동 수준을 판단하였으며, 14개의 자유 진동 모드가 기체 운동 및 진동 수준을 평가하는데 사용되었다. 로터-동체 진동 해석은 일방향 또는 양방향 결합 방법을 통해 수행되었으며 결과는 XH-59A 비행 시험 데이터와 검증하였다. 양방향 결합 해석을 이용한 로터 및 동체 진동 하중은 비행 시험 데이터를 통해 검증했으며, 다양한 작동 시나리오를 통해 로터 허브와 조종석에서 얻은 진동 감소 수준을 분석하였다. IBC는 회전익 항공기의 로터 허브 및 조종석에서의 진동 수준 감소에 매우 효과적이었으며, 다중 고조파 IBC 제어 입력을 통해 회전익 항공기의 전체 진동을 80.6% 감소시키는 것을 확인했다.

Key Words : Coaxial Lift-offset Rotorcraft, Rotor-body Coupling Analysis, Individual Blade Pitch Control, Vibration Reduction

Introduction

High levels of vibration, large noise emissions, and relatively poor aerodynamic efficiencies are some of the major concerns in modern rotorcraft applications. The problem is aggravated with increase in flight speeds, as the edgewise rotor experiences greater differences between incoming air velocities at the advancing and retreating sides of the rotor. Many innovations were devised to overcome the shortcomings with regard to the speed barriers of helicopter flights. One prominent concept is to apply the L.O. mechanism that can maximize the lift generation capacity of the rotor without compromising the aerodynamic deficiencies on the retreating side of the rotor. The roll moment equilibrium is satisfied by the lift produced by a pair of coaxial, counter-rotating rotors that operate with equal and opposite roll moments. The XH-59A is the first aircraft to demonstrate the application of the L.O. mechanism, achieving the maximum forward speed of 240 knots in level-cruise mode[1,2]. However, the test program was terminated because of severe vibrations and high fuel consumption during the flight.

To analyze this problem in detail, the precise modeling of the main rotor and the fuselage system, considering their interactions, is crucial. Such modeling is essential for reliably predicting the vibrations of a full rotorcraft, especially in the cockpit. Rotor-body coupled vibration analysis can be performed using one of the following two approaches: one-way or two-way coupling. In the former approach, the main rotor and fuselage system are examined separately: the vibratory hub loads are computed for an isolated rotor, and then, the load spectrum is used to excite the fuselage (from the hub) for evaluating the vibration at the de-sired locations on the fuselage. The process is unilateral and does not consider any interactions between the rotor and fuselage. In the latter method, the interactions between the rotor and fuselage are considered, and the vibratory loads produced by the rotor are transferred to the fuselage, which in turn changes the motion of the hub via the dynamic response of the fuselage. The changed hub motions (body) modify the hub loads (rotor) accordingly. These interactions are repeated until substantial convergence within a tolerance is reached. Considering the inherent coupling in the problem, the latter approach is regarded a more general approach for the realistic evaluation of rotor-body vibration responses. Nonetheless, a systematic evaluation of the differences in accuracy and efficacy between the two approaches is necessary.

Rotor-fuselage interactions affect the vibrations of both, the rotating and nonrotating systems of a rotorcraft. Previous studies mostly focused on the rotor-body coupling in conventional helicopters[3~5],

while the L.O. rotor system was analyzed using rotors in isolation or with simplified fuselage models[6~13]. So far, there is paucity of comprehensive studies of the loads and vibration behavior of L.O. coaxial rotorcraft, considering the whole rotorcraft system. A few exceptions are the works of Blackwell and Millott[14], and Lee et al.[15]. Blackwell and Millot[14] developed a finite element (FE) model of an L.O. coaxial compound helicopter with a fuselage and active vibration control system (AVCS) installed in the nonrotating system. They demonstrated a reduction in the vibrations of X2TD, which was developed based on the platform of the earlier model, the XH-59A rotor. Lee et al.[15] modeled the fuselage using a one-dimensional (1D) FE stick model with a one-way coupling approach for vibration reduction of XH-59A with individual blade control (IBC) and AVCS. Considerable reduction in vibration was reported, with co-actuation at both rotor (IBC) and fuselage (AVCS). However, the vibratory hub load was not considered with the coupled fuselage effect. Despite the recent attempts, there still remains a gap in research on the rotor-body coupled vibration analysis of L.O. coaxial rotorcraft systems, especially including the application of the two-way coupling approach.

The objectives of the present study are as follows: (1) assessing the accuracy and efficiency of the pre-dictions of rotor-body coupled vibrations for XH-59A flight test data under high-speed cruise condition (the predictions are obtained by the one-way and two-way coupling methods); (2) identifying the rotor-fuselage coupled vibration behavior; and (3) determining the best actuation scenario for minimizing the vibrations using the IBC scheme.

The structure of this paper is as follows. Section 2 describes the methodology used to model the vibration analysis of rotor-fuselage system. The section explains the way the fuselage is represented by a 1D FE stick model, the technique for modeling the aeromechanics of the rotor, and the approach for performing the rotor-fuselage coupling (using one-way and two-way coupling methods). Section 3 presents the validation of the developed model through comparing the results of the one-way and two-way coupling methods. Furthermore, effectiveness on the vibration reduction using individual blade pitch control is discussed. Finally, the paper draws the main findings and conclusions from the present analysis.

SOLUTION APPROACHES

Fuselage FE model

Table 1 summarizes the general properties of XH-59A[1], which is a 5.48-m-long three-bladed coaxial rotor with a vehicle weight of 5,398 kg. For the vibration analysis, the dynamic model of the fuselage was first constructed using MSC NASTRAN. The fuselage can be modeled in different manners, from a simple 1D FE stick model to a detailed three-dimensional FE model. From the viewpoints of efficiency and convenience, a simple 1D FE stick model is used in this study to account for the dynamic motions of the fuselage[4]. Since most of the normal-mode characteristics of the XH-59A fuselage, except the first fuselage symmetric bending mode[1], are not publicly available, values corresponding to conventional helicopters (e.g., UH-60A, AH-1G, and BO-105) were used for the target modes of the fuselage[16~18]. The target frequencies of the fundamental modes of the fuselage are listed in Table 2. The cross-sectional dimension and structural properties of each beam element in the stick model were appropriately assumed and varied to match the target frequencies set for the fuselage structure. The overall vehicle weight and location of the XH-59A are maintained constant during frequency tuning[19]. Fig. 1 shows the final 1D FE stick model built for the present XH-59A fuselage. The model comprises 37 elastic beam FEs, 20 concentrated masses, and a flexible pylon that creates the physical connection between the rotor shaft and fuselage. This flexible pylon mounting system is modeled to match the normal modes of the fuselage. Five multipoint constraints using RBE2 element are used to simulate an elastomeric mounting system, with one bar element installed to model the lift link of the rotor shaft mounting system[18]. The lift link is the primary load path of the vertical force transmitted through the upper and lower parts of the rotor.

Table 1. General properties of the XH-59A rotorcraft.

Property	Value
Number of blades, N_b	3
Number of rotors	2
Radius, R	5.48 m
Root cutout	0.2 R
Mean chord, c	0.36 m
Solidity (single rotor), σ	0.064
Hover tip Mach number, M_{tip}	0.58
Fuselage length	12.4 m
Vehicle weight, W_0	5,398 kg
Nominal rotor speed, Ω_0	344 RPM
Cruise mode rotor speed	338 RPM

Table 2. Comparison of natural frequencies for the target fuselage model.

Fuselage mode	Target, Hz	Present, Hz
1st pylon yaw	3.01	3.01
1st pylon pitch	3.90	3.78
1st vertical bending	5.52–7.94	6.28
1st lateral bending	5.58–7.14	7.6
2nd vertical bending	16.2	16.2
2nd lateral bending	15.3–25.2	16.7

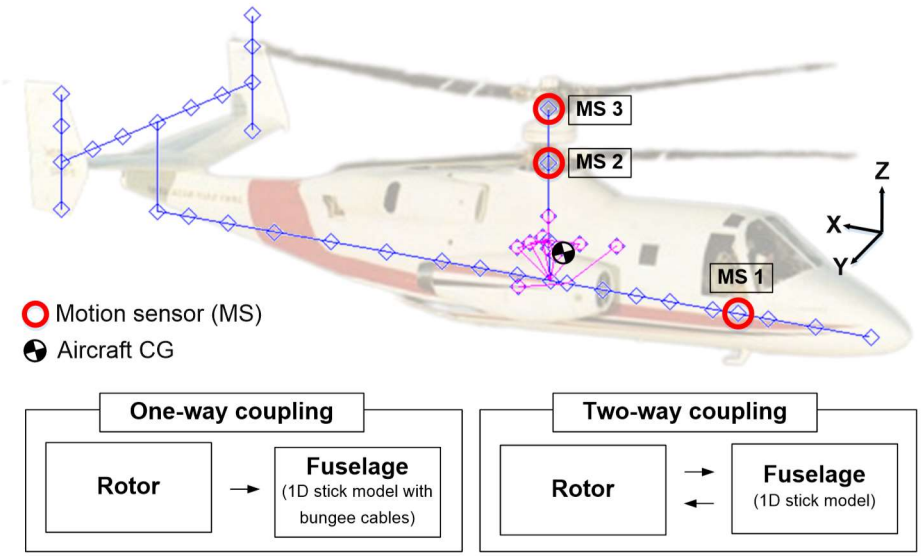

Fig. 1. Rotor–body coupled vibration analysis model for XH-59A.

Rotor-body coupled analysis

Fig. 1 shows a schematic view of the one-way and two-way methodologies for rotor-body coupled vibration analysis. The one-way coupling analysis was mainly conducted in MSC NASTRAN using the direct frequency response analysis solution (SOL 108). The vibratory hub load spectrum obtained from an isolated rotor system with blade passage frequencies (BPFs) of 3 per rotor revolution (3P) were directly applied to the upper and lower hub positions (see Fig. 1). The structural response of the fuselage was then computed as discrete excitation frequencies in a direct response analysis by solving a set of coupled matrix equations of the system. To this end, a ground vibration analysis model of the XH-59A fuselage was constructed using the same set of normal modes as the aforementioned 1D FE stick model. This analysis model included the bungee cables[15] connected to the upper rotor hub and at the empennage as depicted in Fig. 2.

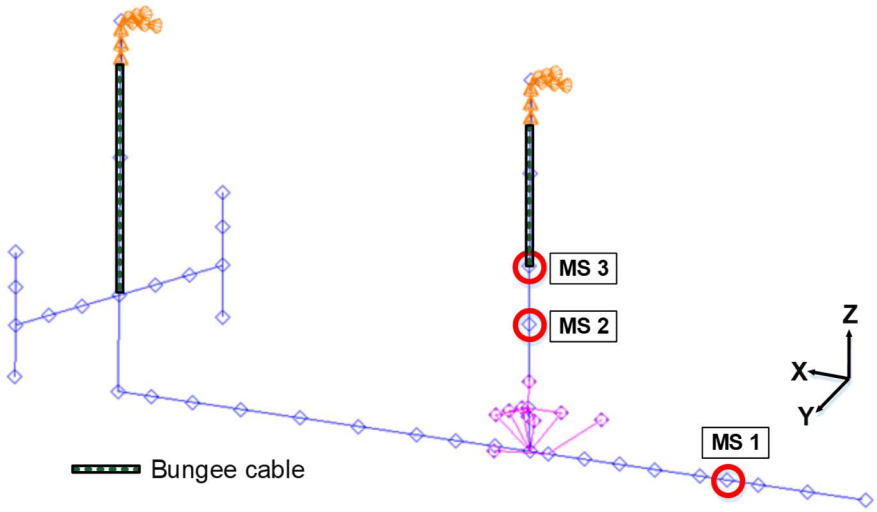

Fig. 2. One-dimensional (1D) ground vibration analysis model of the fuselage.

The two-way coupling analysis was conducted using the comprehensive dynamics analysis code CAMRAD II[20]. The rotor-body coupled analysis was performed by considering the interactions between the hub and airframe motion. To consider the elasticity of the fuselage, the motion loop option in CAMRAD II was used during the vehicle trim process. Fig. 3 illustrates the flow diagram of the analysis process. The trim loop consists of the motion loop itself, which iteratively computes the effect of hub loads on the vehicle motion sensors. To avoid harmonic coupling between the rotor and airframe, the solution was obtained in a nonrotating frame. The elasticity of the fuselage was converted to generalized mass, natural frequency, and eigenvectors from the normal modes analysis results of the 1D FE stick model. The interactions were computed at three collocation points, called motion sensors, as shown in Fig. 1. These motion sensors can capture the elastic behavior of the fuselage. They are located at the lower and upper rotor hubs and at the pilot seat. The rotor hub locations were chosen because of their direct connection to the rotor, which is the main source of vibrations. The fuselage motion was calculated using the linear and angular mode shapes of the individual motion sensors, considering all the forces and moments acting on the rotorcraft.

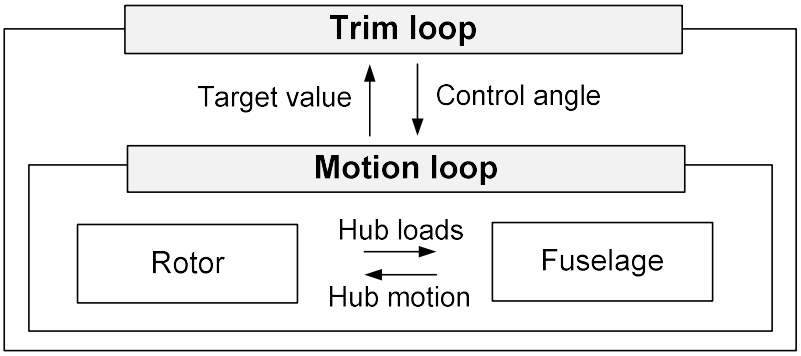

Fig. 3. Schematic view of two-way coupled vibration analysis in CAMRAD II[20].

The governing equation of motion of a rotor–body coupled system is expressed as follows:

$$\ddot{\mathbf{r}} + 2\zeta\boldsymbol{\omega}\dot{\mathbf{r}} + \boldsymbol{\omega}^2\mathbf{r} = \mathbf{f} \tag{1}$$

where $\mathbf{r}$ is the modal degree of freedom (DOF) in generalized coordinates; ζ and $\boldsymbol{\omega}$ are the critical damping ratio and the natural frequency of the normal mode, respectively; and $\mathbf{f}$ is the excitation force in generalized coordinates. In this study, $\mathbf{f}$ is defined as follows:

$$\mathbf{f} = \mathbf{S}^{\mathrm{T}}\mathbf{F} \tag{2a}$$

$$\mathbf{S}^{\mathrm{T}} = \lfloor u_X \quad u_Y \quad u_Z \quad \phi_X \quad \phi_Y \quad \phi_Z \rfloor$$
$$\mathbf{F}^{\mathrm{T}} = \lfloor F_X \quad F_Y \quad F_Z \quad M_X \quad M_Y \quad M_Z \rfloor \tag{2b}$$

where $\mathbf{S}$ is the mode shape vector of the linear and angular mode shapes, and $\mathbf{F}$ is the vibratory hub loads in the nonrotating frame. Since the 1D FE fuselage model considers the rotor as a concentrated mass at the hub center, the inertial loads are included twice in the two-way rotor–body coupled analysis[21]. Therefore, the inertial loads must be eliminated from the generalized force array. The inertial loads are calculated as the mass (masses of the hub and blade) multiplied by the acceleration of the hub. Thus, the fuselage excitation force is expressed as follows:

$$\mathbf{F} = \mathbf{F}_{\mathrm{LH}} + \mathbf{F}_{\mathrm{UH}} + \mathbf{M}_{\mathrm{LH}}\mathbf{S}_{\mathrm{LH}}\ddot{\mathbf{r}} + \mathbf{M}_{\mathrm{UH}}\mathbf{S}_{\mathrm{UH}}\ddot{\mathbf{r}} \tag{3}$$

where the subscripts “LH” and “UH” indicate the terms for the lower rotor hub and upper rotor hub, respectively, and $\mathbf{M}$ denotes the mass matrix. The final form of the governing equation is given as follows:

$$(\mathbf{I} - \mathbf{S}_{\mathrm{LH}}^{\mathrm{T}}\mathbf{M}_{\mathrm{LH}}\mathbf{S}_{\mathrm{LH}} - \mathbf{S}_{\mathrm{UH}}^{\mathrm{T}}\mathbf{M}_{\mathrm{UH}}\mathbf{S}_{\mathrm{UH}})\ddot{\mathbf{r}} + 2\zeta\boldsymbol{\omega}\dot{\mathbf{r}} + \boldsymbol{\omega}^2\mathbf{r} = \mathbf{S}_{\mathrm{LH}}^{\mathrm{T}}\mathbf{F}_{\mathrm{LH}} + \mathbf{S}_{\mathrm{UH}}^{\mathrm{T}}\mathbf{F}_{\mathrm{UH}} \tag{4}$$

where $\mathbf{I}$ is the identity matrix. Since the generalized mass matrix is no longer diagonal, the rotor and body motions are fully coupled in the governing equation. The vibratory hub loads from the rotor are transferred to the fuselage, thereby changing the hub motion according to the mode shapes corresponding to the locations of the motion sensors on the fuselage. The modified hub motion then alters the rotor hub loads. These interactions are repeated until a converged solution is obtained. In both, the one-way and two-way coupling analyses, a critical structural damping ratio of 2% is adopted, considering that the range of the ratio is generally 1%–4%[17].

Comprehensive analysis of the rotor

The rotor-body coupled vibration analysis for the XH-59A rotorcraft under high-speed cruise flight conditions (200 knots and advance ratio μ = 0.53) is performed in CAMRAD II. The structural and aerodynamic analysis models used for the blades are shown in Fig. 4. The blade is discretized using 13 FEs, with one rigid element installed near the blade root. Each FE has 15 DOFs, including three axial, two flap, two lag, and two elastic twist motions. A pitch link with a spring constant of 13,558 N/m is used to model the pitch control input while maintaining the first torsion frequency of the rotor constant. The aerodynamic analysis is based on the ONERA-EDLIN unsteady airfoil theory with C81 table look-up method using a rolled-up tip vortex wake model. The trim analysis consists of six inputs and six targets of the counter-rotating rotor system in high-speed cruise flight. The trim variables include the mean and differential collective pitch angles of the whole rotor and the longitudinal and lateral cyclic pitch angles of each rotor. The goal is to balance the rotor system by adjusting the pitch moments of the lower and upper rotor parts and the difference between the lower and upper rotor hub roll moments, while matching the L.O. and the thrust of the vehicle. The L.O. is defined considering the relation of the lift produced by the coaxial rotor system (L) with the rotor radius (R) and differential roll moments (ΔM_x).

$$\text{L.O.} = \frac{\Delta M_x}{L \cdot R} \tag{5}$$

To simplify the analysis, the fuselage aerodynamic forces, including the rotor drag and auxiliary propulsion system, are assumed to balance themselves. The rotor rotational speed is fixed to 98% of the nominal RPM considering the flight test results[19]. To account for the vibration level of whole aircraft, the vibration index (VI_R) of the rotor hub and body is defined according to the guidelines given in ADS-27A-SP[22]:

$$\text{VI}_\text{R} = \left\{ \alpha_1 \frac{\sqrt{\left(0.5F_X\right)^2 + \left(0.67F_Y\right)^2 + F_Z^2}}{W_0} + \alpha_2 \frac{\sqrt{M_X^2 + M_Y^2}}{W_0 R} \right\} \tag{6}$$

where F_X, F_Y, and F_Z are the hub forces in the longitudinal, lateral, and vertical directions, respectively, and M_X and M_Y are the rolling and pitching moments, respectively. In addition, W_0 is the vehicle weight, and α_i (i = 1,2) ($0 \le \alpha_i \le 1$) are the weighting factors. In the present study, VI_R was calculated using identical weight factors (α_i = 1). Unless otherwise stated, the hub vibration was evaluated using the lowest BPF (i.e., 3P) of the three-blade rotor. The vibration index of a fuselage VI_F is defined by the accelerations evaluated at the pilot seat (MS 1) as follows:

$$\text{VI}_\text{F} = \frac{\sqrt{a_X^2 + a_Y^2 + a_Z^2}}{g} \tag{7}$$

where a_x, a_y, and a_z are the acceleration in the longitudinal, lateral, and vertical directions, respectively, and g is the gravity constant. The overall aircraft vibration $VI_{overall}$ is expressed by combining Eq. (6) and Eq. (7):

$$\text{VI}_\text{overall} = w_1 \text{VI}_\text{R} + w_2 \text{VI}_\text{F} \tag{8}$$

where w_1 and w_2 denote the weighting factors ($0 \le w_i \le 1$). The vibration analysis was performed using equal weight factors ($w_1 = w_2 = 1$). For the performance measure, the effective lift-to-drag ratio (L/D_e) of the rotor is used to evaluate the efficiency of the rotor in forward flight:

$$L / D_e = L \cdot V / (P_i + P_0) \tag{9}$$

where V is the forward speed, and P_i and P_0 are the induced power and profile power of the rotor, respectively.

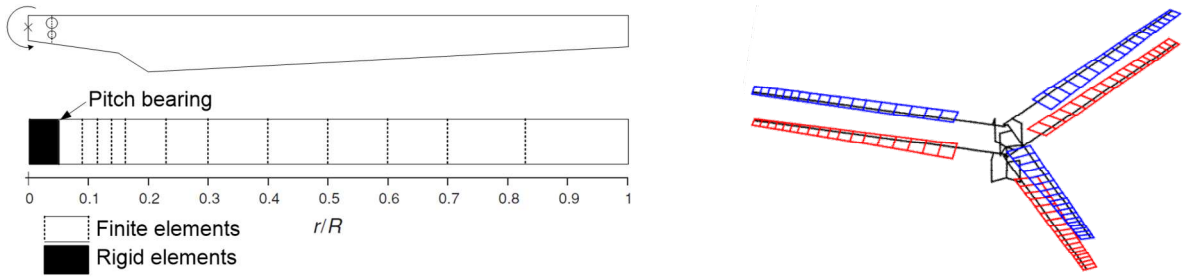

(a) Structural model (b) Aerodynamic model

Fig. 4. Aeromechanics analysis models of coaxial XH-59A rotor.

IBC

The vibratory loads of the rotor are actively suppressed using IBC actuators installed at the pitch link, which is connected to the swashplate. The IBC pitch motions are defined as follows:

$$T(\psi) = A_n \cos(n\psi - \Phi_n) \tag{10}$$

where n is the actuation frequency of the harmonic control pitch input; A_n is the amplitude; and Φ_n is the phase angle. The best actuation deployment scenario for vibration reduction at the rotor hub and pilot seat is sought using a parametric sweep study on amplitudes, frequency, and phase angles in single harmonic actuation. Amplitudes from 0° to 2.0° (increment of 0.5°) were actuated for the present study, and a phase angle sweep was conducted every 30°. The effective actuation amplitude for each actuation frequency was chosen from the parametric results to manipulate the investigation of the multiple harmonic actuations:

$$T(\psi) = \sum_{n}^{N_f} A_n \cos(n\psi - \Phi_n) \tag{11}$$

where frequencies are added up to the frequency contents (N_f) specified by the actuation input. For efficient investigation, the phase sweep was varied by 60° with discrete amplitudes for each actuation frequency.

RESULTS AND DISCUSSION

Validation of the aeromechanics model

The structural dynamics model used for the analysis was validated first against the measured data and earlier predictions[1,2]. Fig. 5 shows a comparison of the natural frequencies of XH-59A blades with the rotor speeds. The predictions show good agreement with the measured data at nonrotating frequencies. Further, compared to the results of previous works, the present predictions are more correlated with the measured data, thereby validating the model of the blade structures and pitch control system of the rotor. Next, the fuselage vibration analysis model with the 1D FE stick representation was validated. Table 2 summarizes the normal-mode analysis results predicted using the 1D stick model with each of the target values set from the conventional data. Notably, all the primary body modes are well within the target frequency ranges, except in the case of the first lateral bending mode (which has an error of 6.4%). In general, these results demonstrate the suitability of the fuselage dynamic model constructed for the rotorcraft vibration analysis. Finally, the convergence behavior of the body normal modes for pilot seat acceleration was investigated using the two-way rotor-body coupled analysis. Fig. 6 shows the convergence results for the acceleration signals (a_X, a_Y, and a_Z) computed at the location of the pilot seat. The cockpit vibration (acceleration) is revealed to be very sensitive to the vibrating

modes, particularly, longitudinal and vertical vibrations (a_X and a_Z), considered in the analysis. According to the convergence study, the lowest 14 modes (up to 9P) are employed in the present coupled vibration analysis.

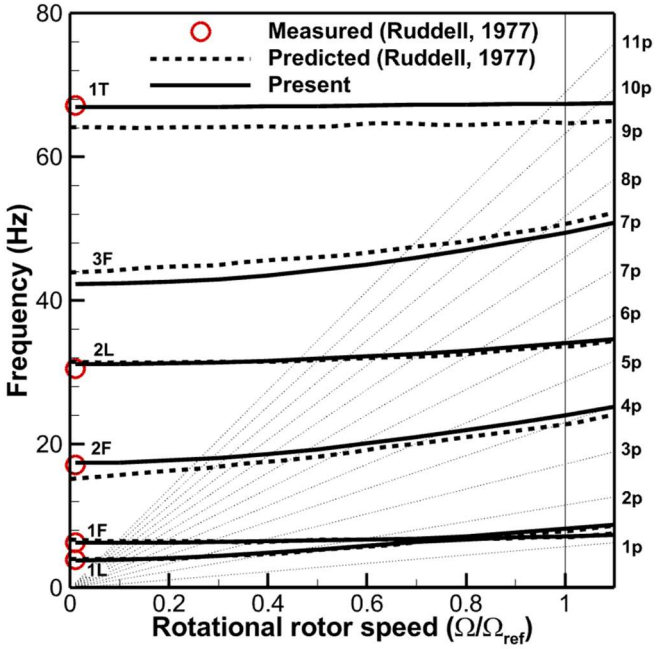

Fig. 5. Comparison of rotating natural frequencies.

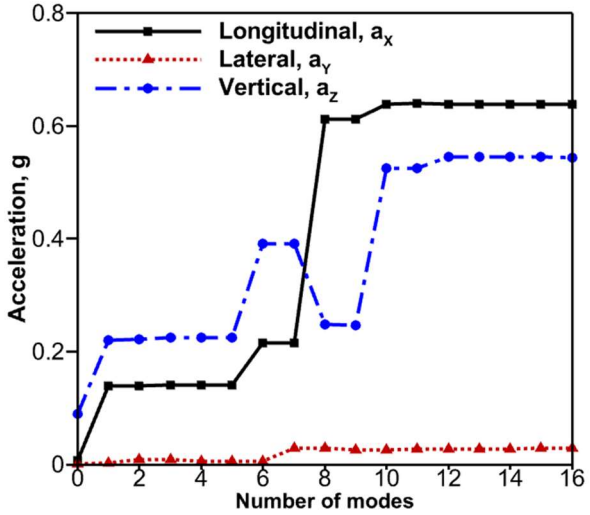

Fig. 6. Convergence behavior on fuselage accelerations at the pilot seat (MS 1).

Validation of rotorcraft vibration levels

Fig. 7 shows the correlation of the results as well as the effect of the rotor–body coupling method on the cockpit vibration (a_X and a_Z) at the pilot seat at flight speeds (120–240 knots). The L.O. is set to 0.2 for all speeds, except for 120 knots (for which the L.O. is 0.1). The measured data and predicted results from previous works[1,15] are used to validate the present analysis. In Lee et al.[15], a one–way rotor–body coupling, similar to the one–way coupling method in this study, was used; the predictions obtained by both of these methods agree well with each other for both acceleration signals, at flight speeds greater than 160 knots. The correlations are less satisfactory at low speeds. The difference in the rolled–up free–wake representations and fuselage dynamics model adopted in each analysis may be the source

of deviations between the predictions. From Fig. 7, it is clear that, compared to the results of the one-way coupling method, the two-way rotor-body coupling results are more closely correlated with the flight test data. Specifically, the longitudinal and vertical vibration levels at the pilot seat obtained using the present two-way coupling show deviations up to 8.4% with respect to the test data at a cruise speed of 200 knots. The deviations increase (up to 20.6%) when the one-way coupling method is used. Note that improved correlation is obtained with an increase in computation time from about 20 min to 52 min because of the hub reactions in the two-way coupling analysis. From the comparison results, the following rotor-body coupled vibration analysis uses the two-way coupling approach for the analyses described hereinafter unless otherwise specified.

The predictions of the blade and hub loads of XH-59A rotor are investigated next. Fig. 8 shows a comparison of the blade flap-bending moments (FBM) at the blade root (0.1R) of the upper rotor, obtained with the present isolated rotor, the rotor body coupled configurations, and the flight test data, with respect to the flight speeds. Because the actual L.O.s or control phase angles for each forward flight speed are not available in the public domain, the present results were computed at L.O. values of both 0.2 and 0.3 and are presented together with the measured data. The present predictions with the selected L.O.'s show only fair correlation with the test data. The rotor-body coupled results have slightly improved correlation with FBM at higher flight speeds, especially for an L.O. of 0.2. Fig. 9 shows a comparison of the vibratory hub pitching moments (M_Y) of the rotor obtained for the same sets of results as those given in Fig. 8. The comparison results clearly indicate that the present rotor-body coupled analysis with an L.O. of 0.2 show excellent correlations with the flight test data, especially for vibratory hub pitching moments. The predicted vibratory roll moments (not shown) show less satisfactory agreements with the test data; however, this has little impact on the prediction because of the cancellation effect of the counter-rotating coaxial rotor system. In this case as well, the influence of including the fuselage on hub vibratory moments marginally improves the correlation with the flight test data.

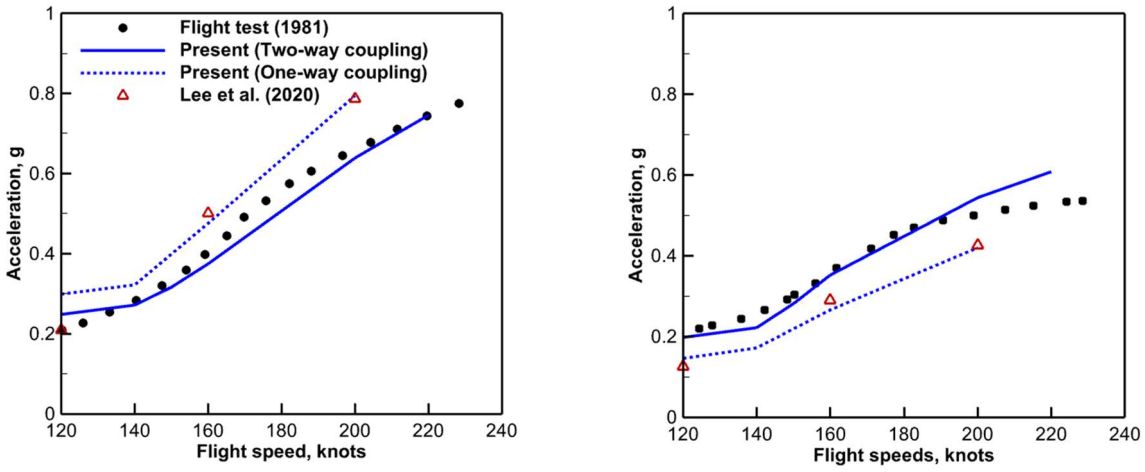

(a) Longitudinal acceleration (a_X) (b) Vertical acceleration (a_Z)

Fig. 7. Comparison of fuselage vibration results at the pilot seat (MS 1).

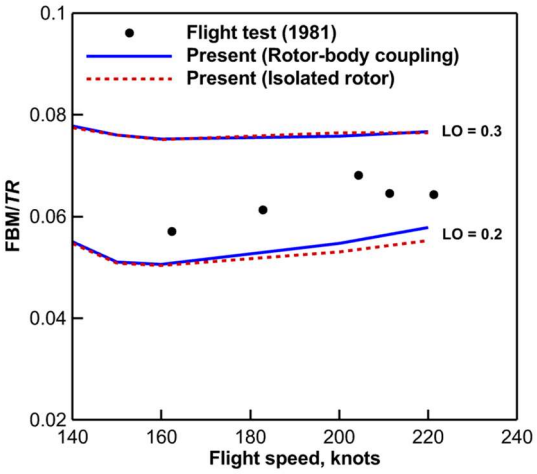

Fig. 8. Comparison of flap-bending moments (p-p) at the blade root (upper rotor).

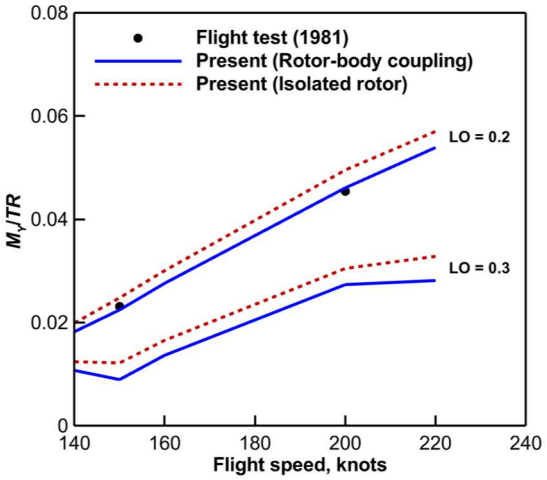

Fig. 9. Comparison of vibratory hub pitching moments.

Fig. 10 shows the effect of the fuselage on hub vibratory forces (F_X, F_Y, and F_Z) with reference to the hub vibration index (VI_R) of the rotor. The predicted hub longitudinal forces (F_X) deviate largely between the present analytic models (i.e., with and without the body) with differences in the other hub forces components. According to a previous work[23], the longitudinal force (F_X) is expected to be larger or at least comparable to the vertical force (F_Z) but no numerical values were reported. The isolated rotor analysis fails to capture this trend, while the rotor-body coupled analysis successfully reproduces it. This result demonstrates the importance of considering the fuselage dynamics in predicting the vibratory hub loads. Notably, despite the large deviation in the longitudinal force, the changes in hub VI_R between the two methods is small because of the increases in the other load components (F_Z) and the scaling effect reflected in defining the index (see Eq. (6)).

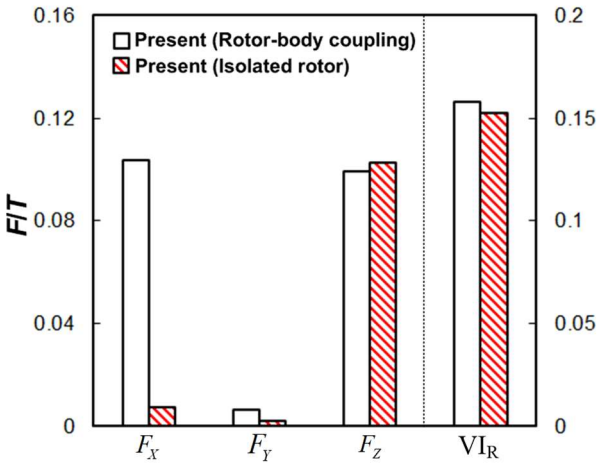

Fig. 10. Comparison of vibratory hub loads (L.O. = 0.2).

Fig. 11 shows a comparison of the effective lift-to-drag ratio of the rotor with the flight test data at different forward speeds. Both the present results show reasonable agreement with the flight test data over the given speed range. Generally, the present results with L.O. = 0.2 have slightly better correlation at low speeds (below 160 knots) and follow the trend of the flight test data as the speed increases. This finding stresses the importance of using L.O. = 0.2 as the desired value when examining the rotorcraft vibration for the XH-59A rotor. Fig. 12 shows the free-wake geometry computed using the present coaxial rotor model in high-speed cruise flight. The rolled-up tip wake geometry is resolved and developed in a well-organized form, indicating sufficient convergence of the free-wake model used in the present analysis.

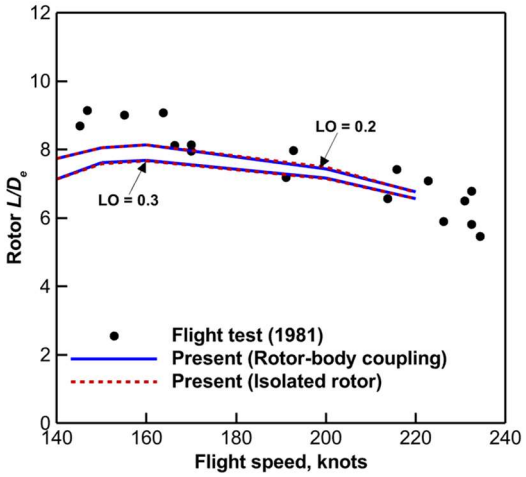

Fig. 11. Comparison of rotor effective lift-to-drag ratios.

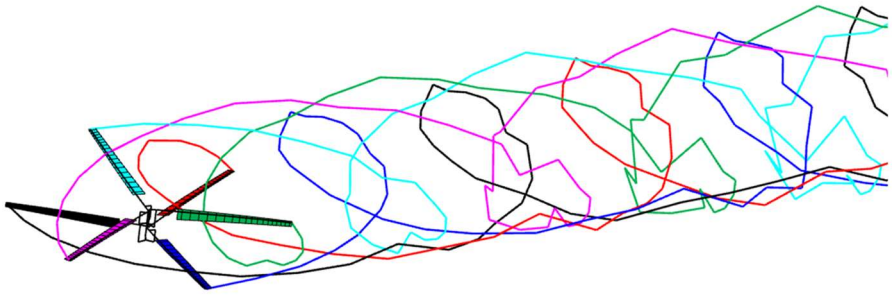

Fig. 12. Computed free-wake geometry of the coaxial rotor model (μ = 0.53).

The above validation study demonstrates that the current two-way coupled vibration methodology, trim strategy, and the detailed aeromechanics modeling are formulated correctly to predict vibrations well, not only at the rotor hub but also at the fuselage locations of the vehicle. The following sections describe active vibration reduction using IBC actuation schemes for the L.O. coaxial rotorcraft. Retrimming is used throughout the rotorcraft vibration analysis.

Vibration reduction using IBC

A parametric sweep study was conducted to investigate the effects of single harmonic actuation with different frequencies (2P, 3P, and 4P) on the vibration response of a two-way rotor-body coupled model. The amplitudes were varied by 0.5° up to 2° half peak-to-peak (p-p), while the phase angles were swept over a rotor revolution at intervals of 30°. Fig. 13 shows the changes in the aircraft vibration ($VI_{overall}$) with different actuation frequencies. The scales in the vertical axis were the same for all results to ensure fair comparison. The IBC actuation with single harmonic inputs has a remarkable impact on decreasing the rotor hub plus the pilot seat vibration of the vehicle. The maximum vibration reduction was about 67% compared to the baseline uncontrolled case. This reduction was obtained at a frequency of 3P with an amplitude of 1.0° and a phase angle of 240° (the yellow circle in Fig. 13(b)). From Fig. 13, the single harmonic actuation results are straight forward to reach the minimum vibration condition. However, the case of multiple harmonic actuation is more complicated because of cases in actuation scenarios with different conditions of vibratory harmonics. To ensure efficiency and convenience, the best amplitudes for each actuation frequency were selected considering the sweep study results for single harmonic actuation. The selected amplitudes were as follows: 2° for 2P, 1.0° for 3P, and 0.5° for 4P inputs.

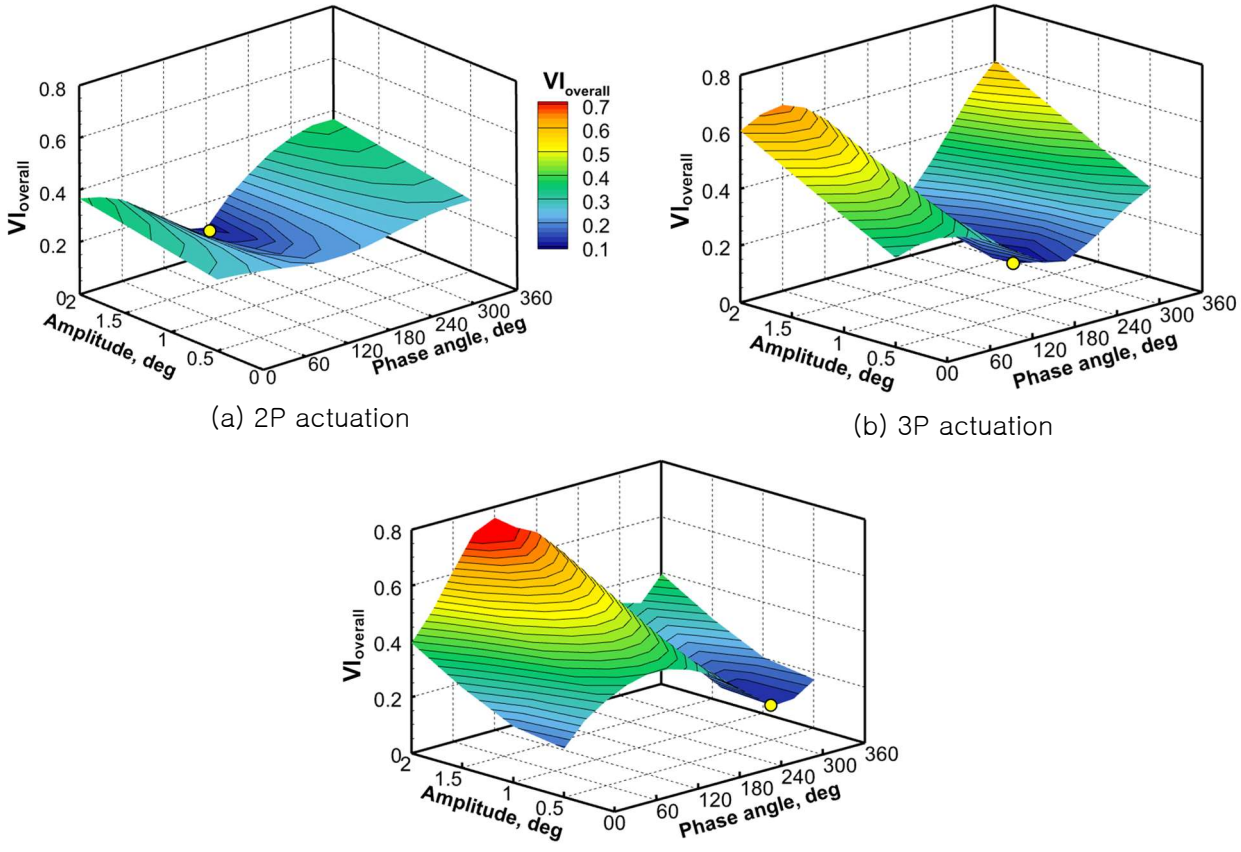

(a) 2P actuation

(b) 3P actuation

(c) 4P actuation

Fig. 13. Variation of overall aircraft vibration $VI_{overall}$ due to individual blade control (IBC) amplitude/phase sweep of the rotor.

Fig. 14 compares the nonvanishing vibratory hub loads components (Fig. 14(a)) and vibration indices (Fig. 14(b) corresponding to the application of different actuation inputs for the coaxial L.O. rotorcraft. The other hub loads components (e.g., F_Y, M_X, and M_Z) become negligible because of the cancellation effects of the counter-rotating rotor. In Fig. 14, the baseline uncontrolled case is also included for reference. Note that each case shown in Fig. 14 represents approximately the minimum vibration conditions for the specific actuation frequency inputs. Both results on hub vibratory loads and vehicle vibration indices demonstrate that an IBC actuation with any harmonics (single or multiple) can be used to reduce the vibrations. Specifically, a multiharmonic IBC with the combined 2P and 4P inputs is the most efficient method for reducing the vibrations at both the rotor and the pilot seat positions. The reduction is approximately 76.6% for the vertical hub force (F_Z) and 80.6% for the overall vehicle vibration ($VI_{overall}$) compared with the uncontrolled case. In general, about 10% more reduction in the vibration level is achieved using the multiple harmonic actuation compared to single harmonic actuation.

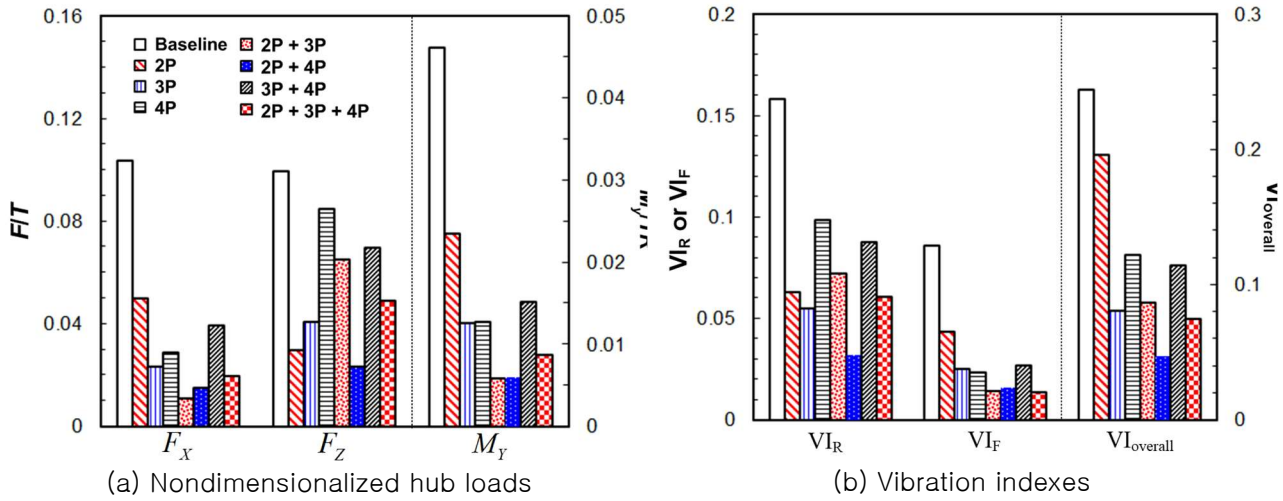

(a) Nondimensionalized hub loads (b) Vibration indexes

Fig. 14. Minimum vibration results obtained for different IBC actuation scenarios.

Fig. 15 shows the representative IBC actuation signals with the best vibration-reduction gains (see Fig. 14) for 3P single and combined 2P and 4P multiharmonic inputs. A comparison of the waveforms of the two best harmonic inputs shows a clear down-up pitch application in the first quadrant and a reversion of the up-down trend in the second quadrant of the rotor disk for both types of actuation. This harmonized behavior of the two signals is observed only on the advancing side; no consistent waveforms are observed at the retreating side. Here, note that the retreating side of the rotor disk plays less important roles in generating the lift for a coaxial L.O. rotor than in the case of the conventional helicopter rotors. The actuation profiles shown in Fig. 15 and their driving mechanism for reducing the vibration of the aircraft are explained further to illustrate the section normal force in the contour format. Fig. 16 shows a comparison of the section normal force distribution between the baseline (uncontrolled) and the best actuation cases, with a time step size of 15°. With actuation (combined 2P and 4P), the section airloads are substantially redistributed, particularly in the advancing side of the rotor disk. The peak values originally at 30° or 160° zones shifted toward 90° azimuth because of the active application of pitch input scenarios. The peak amplitudes also become decreased slightly by the actuation process. In summary, the substantial redistribution and decreased peaks in the section normal force signals contribute to the reduction of the vibration levels of the coaxial L.O. rotorcraft in high-speed cruise flight.

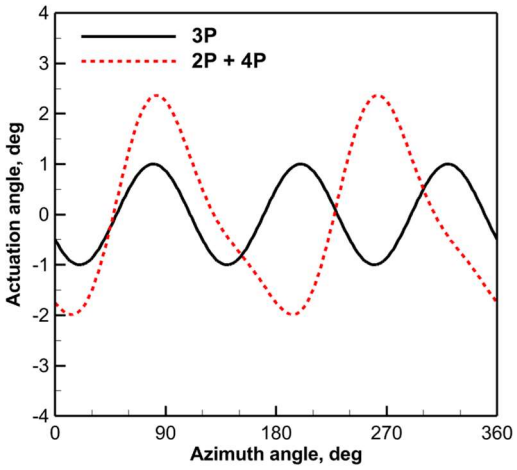

Fig. 15. Selected optimal actuation scenarios for vibration reduction.

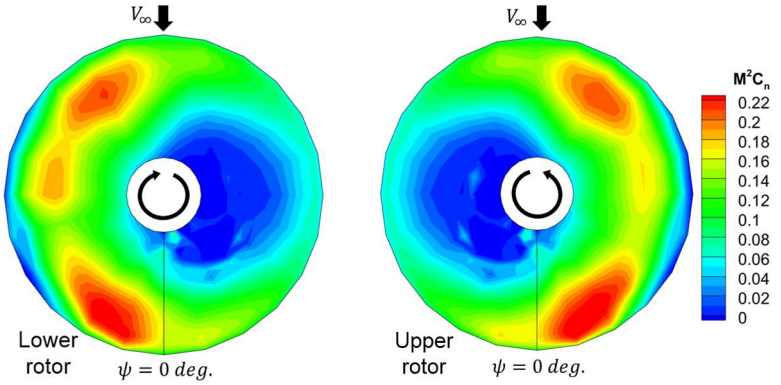

(a) Baseline (uncontrolled)

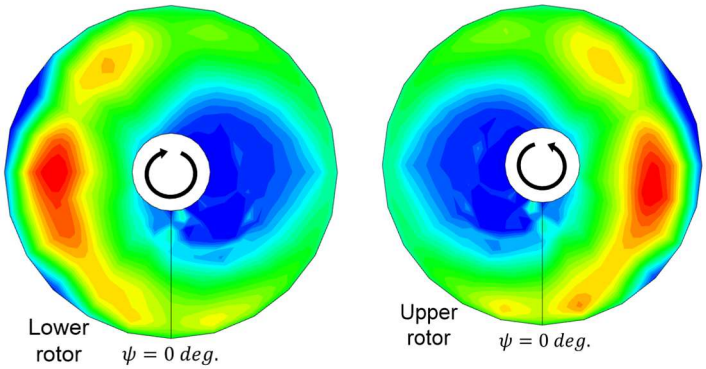

(b) Optimal (2P + 4P)

Fig. 16. Comparison of contour plots showing the section normal force distribution over the rotor disk.

CONCLUSION

In this work, a comprehensive vibration reduction study was performed for an integrated rotor–body system of XH–59A using the IBC technique. A 1D FE stick model of the fuselage was developed based on the natural frequency data of XH–59A and other conventional helicopters. A one–way or two–way coupled vibration model was employed for the rotorcraft vibration analysis, and its effectiveness was evaluated considering the predicted vibration levels obtained at the rotor hub and pilot seat locations, compared with the flight test data. The following conclusions were drawn from this study:

1. The fuselage vibration level predicted at the pilot seat of the aircraft was extremely sensitive to the fuselage vibration modes, especially longitudinal and vertical vibrations. The parametric study demonstrated that at least the first 14 normal modes of the fuselage are needed to obtain sufficient convergence.
2. Compared with the one–way coupled method, the iterative two–way rotor–body coupling provides drastically better the correlation with the test data for both longitudinal and vertical vibrations at the pilot seat with the penalty of increased computational costs (20 min for the one–way method vs. 52 min for the two–way method).
3. The comparison of blade loads (FBM) and vibratory hub moments for the flight test revealed that an L.O. value of 0.2 helps obtain accurate predictions of the general trend of the measured data of the rotorcraft in flight.
4. The influence of the fuselage on the rotorcraft vibration of the L.O. coaxial rotor was crucial for the vibratory longitudinal force signal, despite the seemingly small difference (3.7%) on the overall hub vibration level described in index form (VI_R).
5. IBC actuation with different harmonics for reducing the vibrations at both the rotor hub and the pilot seat locations was demonstrated. The best vibration reduction gains were 67% for single harmonic actuation at 3P frequency with an amplitude of 1° and a phase angle of 240°, and 80.6% for multiple harmonic actuation for a combination of 2P and 4P frequencies. The reduced vibration was attributed to phase shifting toward 90° azimuth zones and alleviation of the peak magnitudes of the section normal forces.

References

[1] A.J. Ruddell, Advancing blade concept (ABC) technology demonstrator, US Army Research and Technology Laboratories, USAAVRADCOM-TR-81-D-5, 1981.

[2] A.J. Ruddell, "Advancing Blade Concept (ABC^{TM}) Development," J. Am. Helicopter Soc. 22 (1977) 13-23.

[3] H. Yeo, I. Chopra, "Coupled rotor/fuselage vibration analysis using detailed 3-D airframe models," Math. Models Comput. Simul. 33 (2001) 1035-1054.

[4] H. Yeo, I. Chopra, "Coupled rotor/fuselage vibration analysis for teetering rotor and test data comparison," J. Aircr. 38 (2001) 111-121.

[5] W. Rex, T. Pflumm, M. Hajek, "UH-60A rotor and coupled rotor-fuselage simulation framework validation and analysis," 45th European Rotorcraft Forum, Warsaw, Poland, Sep 2019.

[6] G. Jacobellis, F. Gandhi, M. Floros, "A physics-based approach to trim optimization of coaxial helicopters in high-speed flight," American Helicopter Society 71st Annual Forum Proceedings, Virginia Beach, USA, May 2015.

[7] J.C. Ho, H.S. Yeo, "Analytical study of an isolated coaxial rotor system with lift offset," Aerosp. Sci. Technol. 100 (2020) 105818.

[8] J.H. Lim, S.S. Shin, Y.J. Kee, "Optimization of rotor structural design in compound rotorcraft with lift offset," J. Am. Helicopter Soc. 61 (2016) 1-14.

[9] J.W. Lim, K.W. McAlister, W. Johnson, "Hover performance correlation for full-scale and model-scale coaxial rotors," J. Am. Helicopter Soc. 54, (2009) 32005.

[10] J. Schmaus, I. Chopra, "Aeromechanics for a high advance ratio coaxial rotor," American Helicopter Society, 71th Annual Forum Proceedings, Virginia Beach, USA, May 2015.

[11] C.G. Cameron, J. Sirohi, J. Schmaus, I. Chopra, "Performance and loads of a reduced-scale coaxial counterrotating rotor," J. Am. Helicopter Soc. 64 (2019) 1-15.

[12] C.G. Cameron, J. Sirohi, "Performance and loads of a lift offset rotor: hover and wind tunnel testing," J. Am. Helicopter Soc. 64 (2019) 1-12.

[13] R. Feil, M. Hajek, J. Rauleder, "Vibratory load predictions of a high-advance-ratio rotor system validated by wind tunnel tests," J. Fluids Struct. 92 (2020) 102764.

[14] R. Blackwell, T. Millott, "Dynamic design characteristics of the Sikorsky X2 technology demonstrator aircraft," American Helicopter Society, 64th Annual Forum Proceedings, Montreal, Canada, Apr. 29-May 1, 2008.

[15] Y.L. Lee, D.H. Kim, J.S. Park, S.B. Hong, "Vibration reduction simulations of a lift-offset compound helicopter using two active control techniques," Aerosp. Sci. Technol. 106 (2020) 106181.

[16] G.R. Howland, J.A. Durno, W.J. Twomey, "Ground shake test of the UH-60A helicopter airframe and comparison with NASTRAN finite element model predictions," NASA-CR-181993, March 1990.

[17] J. Stoppel, M. Degener, "Investigation of helicopter structural dynamics and a comparison with ground vibration tests," J. Am. Helicopter Soc. 27 (1982) 34-42.

[18] H.W. Hanson, "Investigation of vibration reduction through structural optimization, US Army Research and Technology Laboratories," USAAVRADCOM-TR-80-D-13, 1980.

[19] A.J. Ruddell, "XH-59A ABC technology demonstrator altitude expansion and operational tests, US Army Research and Technology Laboratories," USAAVRADCOM-TR-81-D-35, 1981.

[20] W. Johnson, "CAMRAD II: comprehensive analytical model of rotorcraft aerodynamics and dynamics," Johnson Aeronautics, Palo Alto, CA, 1992.

[21] R. Heffernan, D. Precetti, W. Johnson, "Vibration analysis of the SA349/2 helicopter," No. NAS 1.15: 102794 Jan, 1991.

[22] Anonymous, “Standard, aeronautical design standard practice: requirements for rotorcraft vibration specifications, modeling, and testing,” ADS-27A-SP, US Army Aviation and Missile Command, Redstone Arsenal, Alabama, 2006.

[23] A.J. Ruddell, J.A. Macrino, “Advancing Blade Concept (ABC)™ High Speed Development,” American Helicopter Society, Washington, D.C., May 1980.